Journal of Power Sources 194 (2009) 234–242

Contents lists available at ScienceDirect

Journal of Power Sources

journal homepage: www.elsevier.com/locate/jpowsour

Multichelate-functionalized carbon nanospheres used for immobilizing Pt catalysts for fuel cells

P.-L. Kuo*, W.-F. Chen, C.-Y. Lin

Department of Chemical Engineering, National Cheng Kung University, Tainan City, 70101, Taiwan

ARTICLE INFO

Article history:
Received 22 March 2009
Received in revised form 24 April 2009
Accepted 24 April 2009
Available online 3 May 2009

Keywords:
Electrocatalyst
Fuel cells
Methanol oxidation
Carbon
Platinum

ABSTRACT

We have developed a covalent/coordinate strategy to immobilize Pt nanocrystals (average diameter 3.5 nm) on multichelate-functionalized carbon nanospheres (CNS). The method involves the covalent grafting of triethylenetetramine onto the CNS' surface and the coordination of well-structured ethylenimine chains to Pt ions or atoms. The Pt–CNSs interface is probed with X-ray photoelectron spectroscopy to elucidate the nature of the chemical binding of ethylenimine to Pt. The Pt particle deposition can be easily controlled; to form separated and uniform Pt nanocrystals, or densely loaded Pt particles, depending on the molar ratio of Pt to amine groups. The Pt particle layer covered carbon exhibits significantly higher activity toward methanol oxidation (0.75 A mg^{-1} cm^{-2}) than commercial E-TEK 40% Pt loaded carbon with the corresponding data of 0.51 A mg^{-1} cm^{-2}.

1. Introduction

Fuel cells have recently drawn a great deal of attention due to their potential for various stationary and mobile applications [1–3]. Generally, metal catalysts for fuel cells are supported on conductive materials with high surface areas [4,5], which allows the catalysts a higher degree of dispersion. Different methods have been used to prepare carbon-supported catalysts for fuel cells, such as impregnation [6], surfactant or polymer stabilization [7] and microwave-assisted process [8], all of which enable high catalyst dispersion and synergic effects. Impregnation and the polyol process are simple and suitable for large-scale production; however, they are not adequate from the view point of simultaneously offering high dispersion of metals on carbon and high quantity of effective Pt sites [9], and furthermore, the microporosity of the carbon support would limit the accessibility of deposited Pt to the fuel (e.g. methanol). Although surfactant stabilization has been reported to achieve well-dispersed Pt particles over the supporting carbon [10], substantial aggregation of the particles occurred at a high catalyst loading percent (40% or higher). Hence, accomplishing the synthesis of such nanoparticles with good dispersion rates on the supporting materials remains a challenging and tedious work.

Functionalization of the carbon materials is an efficient way to immobilize catalyst particles on the surface and retain indispensable properties, such as the dispersion and stabilization of the catalyst. Functionalization can tailor the structure and properties of the surfaces to facilitate the preparation of innovative carbon-based nanodevices and composites. The addition of organic functionality to carbon-based materials is of particular interest as a desirable and simple means of improving conventional properties, and as a route to obtain new nanomaterials [11–14]. Such organic/inorganic composites can be assembled by the methodologies of noncovalent mixing/adsorption [15] and covalent linkage [16–21]. Generally, covalent functionalization makes the resulting composite more stable and more controllable.

There are two main methodologies for the covalent attachment of organic substances to the surface of the carbon materials, which are defined as "grafting to" and "grafting from" approaches. The former involves attaching either 'in-house' synthesized or commercially available macromolecules onto a carbon surface followed by an end group transformation. A prerequisite of this method is that the macromolecules must possess suitable reactive functional groups or radicals. To-date, many organic molecules, e.g. polymers [22–24], oligomeric and polymeric species including poly(ethylene glycol) (PEG) blocks [25], as well as dendrimers [26], and hyperbranched polymers [27], have been successfully bonded onto carbon materials.

In this work, a hydrophilic multichelate molecule (triethylenetetramine, TETA) was attached to the convex surfaces of carbon nanospheres (CNS) by the "grafting to" approach. Ethylenimine is a functional specialty monomer of both academic and commercial interest. It has been utilized to develop pseudo-dendritic polymers and dendron-like surfactants for metal ion recovery [28], anti-wear [29], and stabilization of metal nanoparticles [30,31]. Thus, it would

* Corresponding author. Tel.: +886 6 2757575 62658; fax: +886 6 2762331.
E-mail address: plkuo@mail.ncku.edu.tw (P.-L. Kuo).

0378-7753/$ – see front matter © 2009 Elsevier B.V. All rights reserved.
doi:10.1016/j.jpowsour.2009.04.059

be fascinating if such a chelating oligomer could be grafted onto carbon materials, since the high density of amino groups and the carbon nanostructure would provide a versatile platform to design and construct novel nano-objects.

Chen et al. [32] have shown that ethylenimine chains can stabilize Pt nanocrystals (of approximately 3 nm in diameter) by the steric hindrance effects exerted by well-structured chelating hydrophiles, which serve as powerful protecting agents for the nanoparticles in the preparation of carbon-supported Pt catalysts. A number of strategies have been used to disperse nanoscopic Pt particles on carbon materials. Particularly interesting is the approach that involves functionalization of the carbon materials to create surface functional groups, such as carboxyl (–COOH) [33], polyhydroxyl methacrylate [34] and mercaptan [35]. We evaluated the ethylenimine-functionalization of carbon in order to immobilize Pt nanocrystals onto CNSs. The resulting multichelate-grafted CNSs were used to sequester a Pt precursor for the purpose of preparing novel CNS/metal hybrid composites.

2. Experimental

2.1. Materials

FW-200/200B active carbon with a BET surface area of 550 $m^2\,g^{-1}$ was purchased from Degussa. Hexachloroplatinic acid ($H_2PtCl_6{\cdot}6H_2O$) was obtained from Alfa Aesor, while the Nafion solution (5 wt.%) was from Du Pont. Carbon paper (Toray, 50 wt.% wet-proofing) and commercial Pt catalysts (20 wt.%) were provided by E-TEK. Other chemicals, including nitric acid (HNO_3, 69.5 wt.%), thionyl chloride ($SOCl_2$), triethylenetetramine ($H_2NCH_2CH_2NHCH_2CH_2NHCH_2CH_2NH_2$), sodium hydroxide (NaOH), sodium borohydride ($NaBH_4$), methanol (CH_3OH), sulfuric acid (H_2SO_4) and isopropyl alcohol ($CH_3CHOHCH_3$, IPA), were obtained from Aldrich. All materials were used as received without further purification, and all aqueous solutions were prepared using deionized water purified through a Milli-Q system.

2.2. Synthesis of ethyleimine-functionalized carbon

The CNS, Degussa FW-200/200B, was pretreated with HNO_3 for 6 h at 80 °C. After cooling to room temperature, the reaction mixture was washed with deionized water until a pH of 7 was obtained, subsequent to which the product was dried under vacuum at 60 °C for 24 h, yielding carboxyl-functionalized carbon. The prepared carboxyl-functionalized carbons were refluxed with excess neat thionyl chloride at 65 °C for 24 h. The residual $SOCl_2$ was removed by distillation, giving acyl chloride-functionalized carbons. The acyl chloride functionalized carbons were immediately reacted with excess TETA at 120 °C for 48 h. Unreacted TETA was removed by washing with ethanol and deionized water until the filtrate became clear, yielding the ethylenimine-functionalized CNSs, ***C***-$(EI)_3$.

2.3. The immobilization of Pt nanocrystals on C-$(EI)_3$

The ***C***-$(EI)_3$-supported Pt catalysts were prepared by mixing H_2PtCl_6 aqueous solutions with a suspension of ***C***-$(EI)_3$ (using [Pt]/[N] ratios of 0.065, 0.13, 0.26, 0.52 and 0.78, respectively). The solutions were stirred vigorously and subjected to ultrasonification for 1 h. The different nominal metal loading percentages were labeled as ω_n (wt.%). In this study, the nominal metal loading percentages were: 5, 10, 20, 40 and 60 wt.%, respectively. The real loading percentage was labeled as ω_r (wt.%), and measured by TGA. The pH value of the prepared colloid was adjusted to approximately 9.2 by the addition of 0.1 M NaOH. Sodium borohydride was added at room temperature with vigorous stirring to reduce the Pt ions. The molar ratio of $NaBH_4$ to H_2PtCl_6 was 5. Then, after separating the solid residue and solvent, the resulting solids were washed with copious amounts of distilled water to remove excess Cl^- by centrifugation, with the material finally being dried in an oven at 90 °C for 6 h.

2.4. Characterization

The extent of functionalization, as measured by the presence of carboxylic acid groups on the HNO_3 treated activated carbon was determined by a back-titration method [36]. The amount of carboxyl groups on the activated carbon was determined by adsorption neutralization with $NaHCO_3$. A 500 mg sample was equilibrated with 25 mL of 0.1N $NaHCO_3$ for 24 h, and then 25 mL of 0.1N HCl was added to aliquots and back-titrated with 0.1N NaOH after boiling off the CO_2. The concentration of amino groups on ***C***-$(EI)_3$ was determined by potentiometric titration by the method proposed by Siggia and Hanna [37] in which the total amine was determined by direct titration of the polymer using 1:1 isopropanol–ethylene glycol as a solvent. The neutralization points of the individual titration were determined from the inflection points of apparent pH versus volume of hydrochloric acid plots. Potentiometric titrations for the determination of the amine value as well as back-titrations for carboxylic acid groups were carried out by an autotitrator of TOA Electronics Ltd. (AUT-301).

X-ray photoelectron spectroscopy (XPS) measurements were carried out with a VG Scientific ESCALAB 210 electron spectrometer using Mg-K_α radiation under a vacuum of 2×10^{-8} Pa. Narrow scan photoelectron spectra were recorded for the C 1s, O 1s and N 1s regions and analyzed by deconvolution to estimate the surface oxidation states of the composites.

The morphologies and size distributions of the catalytic materials made were characterized by transmission electron microscopy (TEM) using a JEOL JEM-1200CX microscope operating at 120 kV. Specimens were prepared by placing a drop of the colloidal dispersion onto 200-mesh copper grids coated with an amorphous Formvar carbon film and dried overnight at room temperature in a vacuum oven before introducing the grid into the microscope. The mean diameters of the nanoparticles was calculated by counting 200 particles with a loupe from magnified (×200,000) TEM images.

X-ray powder diffraction (XRD) was performed on a Rigaku RINT2100 X-ray diffractometer with Cu-K_α radiation (λ = 0.1524 nm) operated at 40 kV and 40 mA by placing the sample powders onto glass slides.

A CHI-608A potentiostat/galvanostat and a conventional three-electrode test cell were used for electrochemical measurements. A Pt wire and saturated calomel electrode (SCE) were used as the counter and reference electrodes, respectively. The working electrode is a thin layer of Nafion-impregnated catalyst cast on a 1 cm^2 vitreous carbon disk. The catalyst powder was dispersed in a small volume of water, then adding isopropanol and stirred vigorously for 1 h. Then 2.5 wt.% Nafion® solution was added into the slurry by keeping the weight ratio of catalyst to Nafion® (dry) at 5:1. After ultrasonic mixing for 1 h, the resulting ink was spread on a carbon disk and dried under vacuum at 60 °C for 3 h.

3. Results and discussion

The synthesis of multichelate-functionalized CNSs involves the three main steps that are shown in Fig. 1. First, carboxyl-rich CNSs were prepared by oxidizing Degussa FW-200 carbon black (primary particle size ~20 nm) with 60% HNO_3 to produce a significant number of carboxyl groups on the CNS surfaces, these were then reacted with $SOCl_2$ to produce acyl chloride-functionalized CNS. TETA was grafted to the CNS surface by the reaction between the acyl chlo-

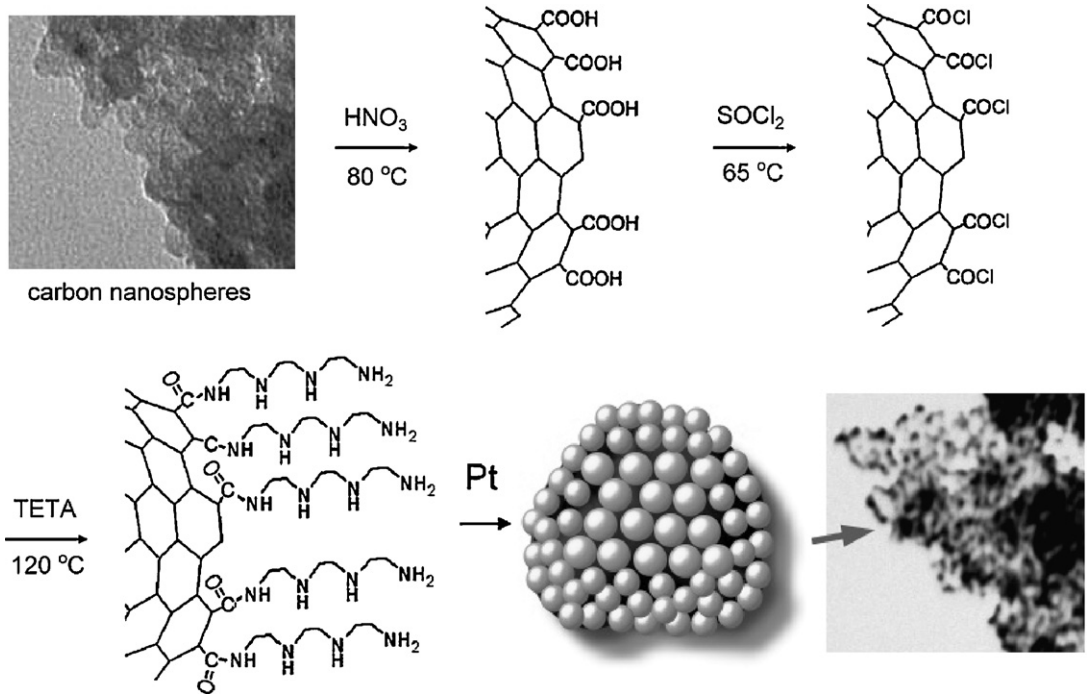

Fig. 1. Illustration of the synthesis process comprising the functionalization of CNS and immobilization of densely-loaded Pt nanoclusters.

ride and the amine groups. These grafted ethylenimine chains, in turn, serve as the chelate sites for Pt immobilization. The so-called "graft-to" technique is a covalent functionalization; which, in contrast to noncovalent functionalization, enhances the deposition of Pt nanoparticles on the exterior surface of CNS, thereby preserving their electrochemical activity.

The strategy we adopted permits the assembly of pre-synthesized nanoparticles as well as the metal precursors, required by each specific application. Pt-covered CNSs with different Pt loadings can be obtained by controlling the Pt:CNS concentration ratio during the deposition process. The ethylenimine chains stabilize the Pt nanoparticles through steric effects and thereby serve to immobilize Pt on the CNS surface to form a dense particulate layer structure.

3.1. Synthesis of multichelate-functionalized CNSs

Some surface functional groups such as hydroxyl and carboxyl groups on carbon materials are known to be generated through oxidation [36]. As shown in Table 1, the amount of carboxyl groups on the carbon was determined, by a back-titration method, to be 1.43 mmol g^{-1} carbon. Assuming that one TETA molecule reacts with one acyl chloride residue, a nominal total amine value of 3.63 mmol g^{-1} is obtained. The experimental total amine value on the CNS surface, as determined by the back-titration method, was 3.86 mmol g^{-1}, which is close to the nominal amine values.

To elucidate the surface states of these CNSs after modification and to correlate the surface states with metal deposition, XPS was used. Our experimental results confirmed the existence of the surface functional groups on these modified materials. The XPS results clearly show that the CNSs treated with HNO_3 (Figs. 2b and 3b) have enhanced O 1s peaks and possess significant amounts of oxidized carbon in comparison with untreated samples (Figs. 2a and 3a). In pristine CNS, graphitic carbon at 284.6 eV is detected and only a small amount of oxygen is found, which can be considered as an

Table 1
Characteristic data for ethylenimine-functionalized CNSs.

Carboxyl values (mmol g^{-1})	Total amine values (mmol g^{-1})	
	Nominal value[a]	Experimental value
1.43	3.64	3.86

[a] The thermal decomposition temperature, defined as the temperature at 10 wt.% weight loss.

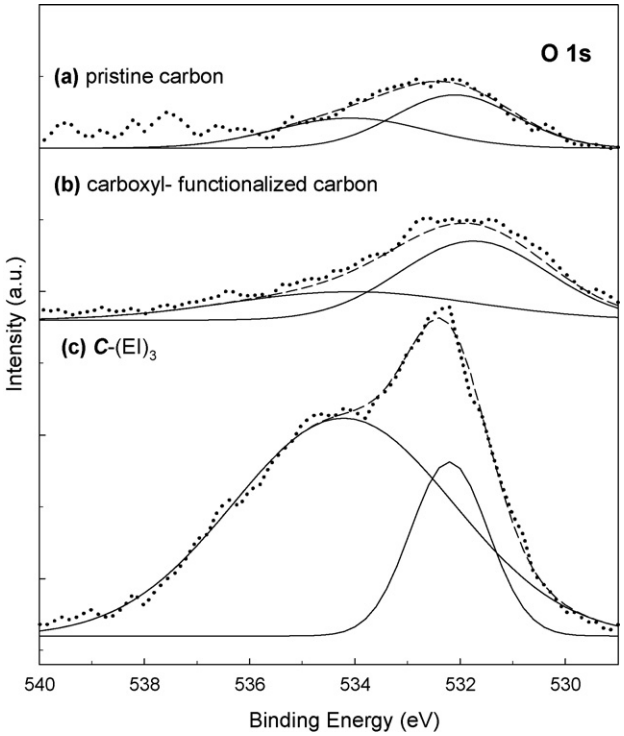

Fig. 2. The XPS spectra of the O 1s regions (a) Degussa carbon, (b) carboxyl-functionalized carbon and (c) ***C***-$(EI)_3$. (●, raw data; – fit data; – – –, deconvoluted data).

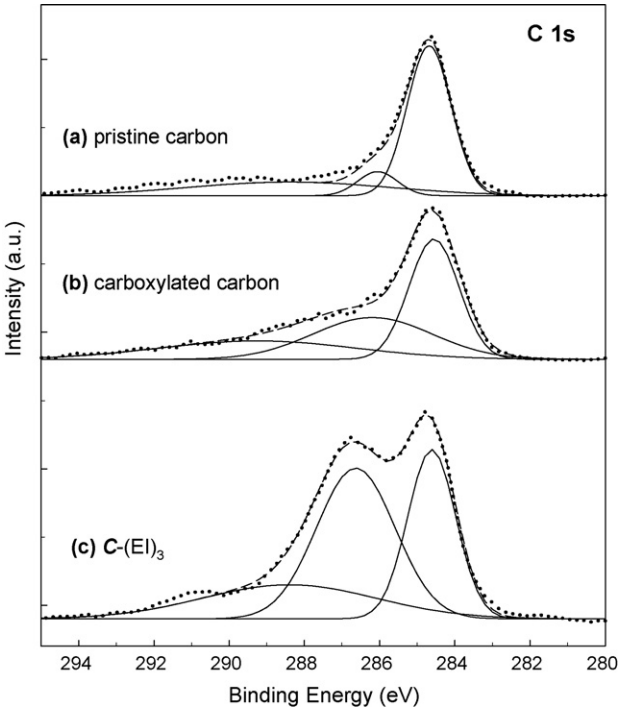

Fig. 3. The XPS spectra in the C 1s regions of (a) Degussa carbon, (b) carboxyl-functionalized carbon, (c) ***C***-$(EI)_3$. (●, raw data; –, fit data; – – –, deconvoluted data).

adsorbed oxygen species. These results imply that a high density of oxygen-containing species is produced on the surface of the CNS after oxidation. Furthermore, the curves of carboxyl-functionalized CNS and ***C***-$(EI)_3$ were found to consist of two nearly superimposed signals. Referring to the XPS studies of surface-oxidized carbon fibers, the present fitting of the O 1s peaks suggests the presence of a carbonaceous species, such as –C═O, or an ether-like species at 532.2 eV and the carboxylic or ester-like groups at 534.1 eV [38], while the presence of C 1s peaks at 286.5 and 288.5 eV results from –C═O and carbonyl carbons such as COOH and COOR, respectively (Fig. 3b) [39].

It can be seen in Fig. 2c that the 534.1 eV peak increases markedly after grafting TETA onto the CNS surface. This increase is attributed to the amide linkage; the peak position of which is coincident with that of the carboxylic groups. In the C 1s spectra (Fig. 3c), this amide linkage shows an intense peak at 286.5 eV. Derived from the N 1s line shown in Fig. 4a, are two peaks, which appear at 399.1 and 400.5 eV, respectively. These demonstrate the presence of free amine groups [40] and the protonated ammonium ions [41]. The inset of Fig. 4a is the N 1s line of pristine CNS which indicates that no nitrogen species. In Fig. 4b, another chemically different N entity can be identified at 397.1 eV in the sample of Pt loaded ***C***-$(EI)_3$. This additional peak can be assigned to the Pt–N bonding, derived from the interaction between the Pt nanoparticles and the amines on ***C***-$(EI)_3$ [42].

3.2. Immobilization of Pt nanocrystals on C-(EI)$_3$

The loading percentage of the Pt nanoparticles onto the ***C***-$(EI)_3$ was altered by changing the concentration ratio of the Pt precursor and the amino functionality in the colloidal solutions. In our study, the [Pt]/[N] ratio was variously assigned as 0.065, 0.13, 0.26, 0.52, or 0.78 (samples: **A**, **B**, **C**, **D** and **E**, respectively). These [Pt]/[N] ratios are equal to: 5, 10, 20, 40 and 60 wt.% of the nominal Pt loading percentages (ω_n). To create a stable Pt/***C***-$(EI)_3$ interface, the initial complexation of the Pt(IV) precursor with the CNSs was crucial for successfully depositing finely dispersed Pt nanoparticles. Pt was immobilized on the surface of ***C***-$(EI)_3$ by reducing the bound Pt(IV) ions with $NaBH_4$ as described in the Section 2. The resulting morphologies of the Pt/***C***-$(EI)_3$ composites were investigated by TEM in terms of the quality of the dispersion and the quantity of the nanoparticles. The TEM images of these metal carbon composites (Fig. 5) indicate that the deposition of well-dispersed Pt as small metal clusters on the surface of the CNSs is achieved when they are functionalized with TETA. Attempts at depositing finely dispersed and densely loaded, ~3.5 nm diameter Pt clusters were successful at [Pt]/[N] ratios of 0.52 and 0.78, indicating that ethylenimine groups provide an effective steric stabilization to prevent Pt nanoparticles from aggregating. On the other hand, the lower loading samples **A**, **B** and **C** resulted in isolated Pt clusters deposited on the CNSs. It is interesting to note that, for these lower loading samples, the particle size remains nearly constant at about 3.5 nm (Table 2), while the quantity of Pt particles decreases. A rational explanation for this uniform size of 3.5 nm is that there is an optimal size for the nanocrystals that allows the most stable packing arrangement for the capped ethylenimine chains.

In order to estimate the grain size of the densely packed Pt nanoparticles, the powder XRD patterns of these Pt-immobilized CNSs were recorded, as shown in Fig. 6. The diffraction peaks observed at 20–25° in all the XRD patterns are due to the (0 0 2)

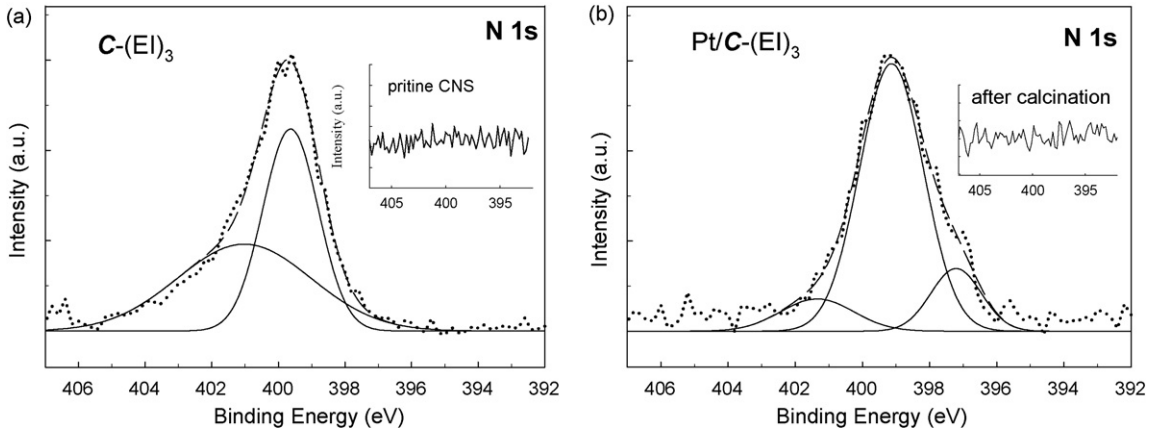

Fig. 4. The XPS spectra of the N 1s regions (a) ***C***-$(EI)_3$, (b) Pt/***C***-$(EI)_3$ (●, raw data; –, fit data; – – –, deconvoluted data). The inset of (a) shows the N 1s line of pristine CNS. The inset of (b) is Pt/***C***-$(EI)_3$ after calcination under N_2 at 300 °C for 10 h.

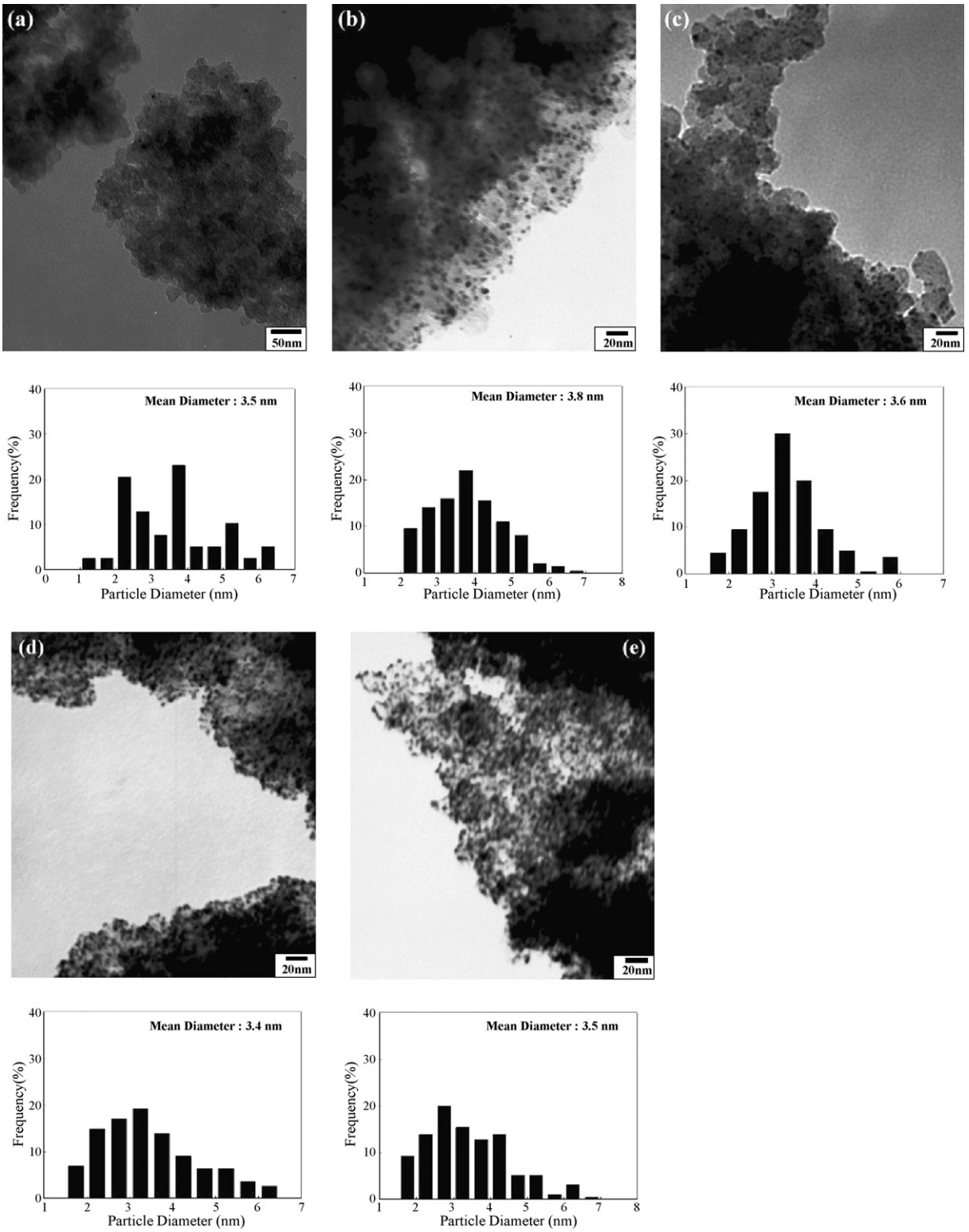

Fig. 5. TEM images and corresponding size histograms of the Pt nanoparticles after depositing on ***C***-$(EI)_3$ with different [Pt]/[N] ratios: (a) 0.065, (b) 0.13, (c) 0.26, (d) 0.52 and (e) 0.78.

plane of the hexagonal structure of the Degussa carbon. The characteristic diffraction peaks at 39°, 46°, 67° and 81° are designated to the Pt {1 1 1}, {2 0 0}, {2 2 0} and {3 1 1} facets of the face-centered cubic (fcc) crystal structure, respectively [43]. The grain sizes were obtained by measuring the broadening of the {1 1 1} peaks and applying the Scherrer equation [44]. Except for sample **A**, in which the width was not able to be calculated, the particle sizes (diameters) found for samples **B**, **C**, **D** and **E** were 3.8, 3.1, 3.2, and 3.4 nm, respectively, which are close to the diameters obtained by TEM images. These results indicate that although the Pt clusters were densely immobilized on the CNS surface for samples **D** and **E**, these Pt particles still maintained their small size and were mainly composed of single crystals with well-developed {1 1 1} planes.

Table 2
Loading percents and the average particle sizes of the Pt/***C***-$(EI)_3$ composites.

Sample	[Pt]/[N]	ω_n (wt.%)[a]	ω_r (wt.%)[b]	χ (ω_r/ω_n, %)[c]	d (nm)[d]
A	0.065	5	–	–	3.5
B	0.13	10	8.6	86	3.8
C	0.26	20	16.6	83	3.6
D	0.52	40	27.2	68	3.4
E	0.78	60	37.5	63	3.5

[a] Nominal Pt loading weight percent.
[b] Real Pt loading weight percent.
[c] Efficiency of Pt loading.
[d] Mean particle size of the Pt nanoparticles on ***C***-$(EI)_3$ calculated by calculated by counting 200 particles with a loupe from magnified (×200,000) TEM images.

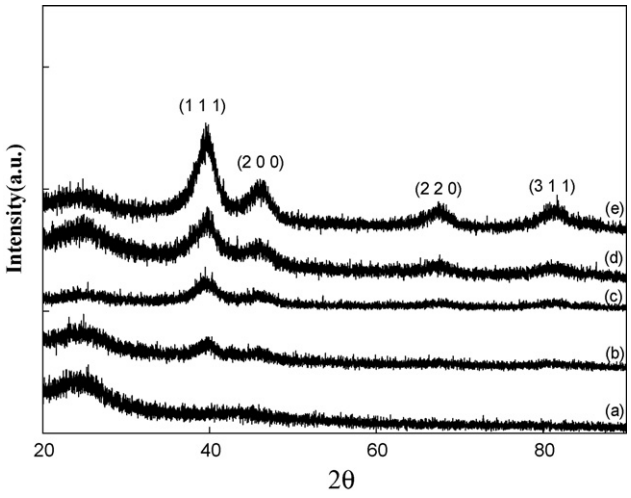

Fig. 6. X-ray diffraction patterns of the Pt/***C***-$(EI)_3$ composites with different [Pt]/[N] ratios: (a) 0.065, (b) 0.13, (c) 0.26, (d) 0.52 and (e) 0.78.

3.3. Loading behavior of Pt nanocrystals

The real loading percentages of the Pt/***C***-$(EI)_3$ composites were analyzed by measuring the residual percentages in TGA by using air to decompose all the carbonaceous components. Fig. 7a shows the TGA thermograms of samples **C**, **D** and **E** measured in air. There are three apparent decreases in the sample weights shown in the thermograms. The first step ranged from 50 to 150 °C and was attributed to the evaporation of the hydration water. A second apparent weight loss was produced between 200 and 360 °C. In addition to the decomposition of the ethylenimine groups on ***C***-$(EI)_3$, as discussed above, in the TG thermogram of ***C***-$(EI)_3$ in N_2, this weight loss also involved the oxidation of surface carbonaceous species such as –COOH, and –COH groups. The temperature of the maximum decomposition rate observed during this step increased from 302 to 348 °C when the [Pt]/[N] ratio was increased from 0.26 to 0.78. We believe that the immobilized Pt clusters on the CNS surface stabilized the amide linkage and the ethylenimine chain through Pt–N coordination bonding, as discussed in the N 1s XPS results. Above 360 °C, there was an appreciable loss of mass, which may correspond to the decomposition of graphitic or high crystalline carbon.

After reaching a steady state, the thermograms remained stable. It can be assumed that all the carbon had been burned away at the high temperature employed, i.e. 850 °C. The real Pt loading percentages, (ω_r), were calculated from the residue values by subtracting the weight of hydrated water from the total weight. The losses were 16.6, 27.2 and 37.5 wt.% for samples **C**, **D** and **E**, respectively (Table 2). The Pt loading behavior is illustrated by plotting the nominal loading percentage value versus the real loading percentage, as shown in Fig. 7b. It is interesting to note that the slope of the ω_r line decreased after ω_n became higher than 0.26. This observation can be explained by the complexing ability and the reversible equilibrium inherent in the coordination process of the Pt(IV) ions and the unpaired electrons of the amino groups on *C*-$(EI)_3$. As reported by Crooks et al. [45] the coordination between Pt and the amine nitrogen forms the most stable octahedral structure when the complexing ability is three (i.e. [Pt]/[N] = 0.33). For a [Pt]/[N] ratio lower than 0.33 (in the present case [Pt]/[N] = 0.13 and 0.26), most of the Pt(IV) ions should be complexed by the amino groups. When the [Pt]/[N] ratio was higher than 0.33 (i.e. samples **D** and **E**), the positive charges of the complexed Pt(IV) on the CNS surface induced an electrostatic repulsion toward the Pt

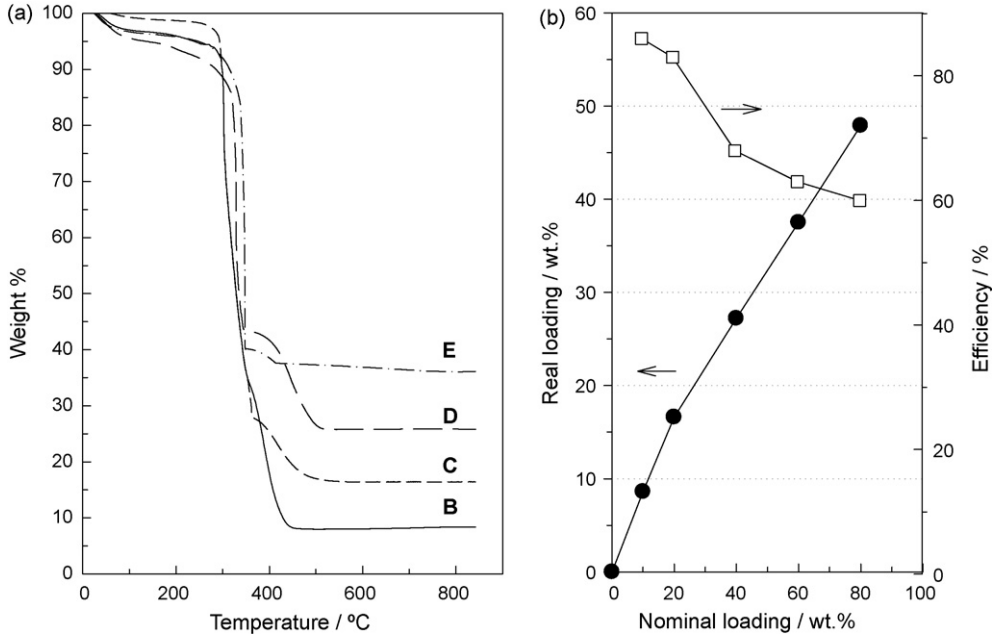

Fig. 7. (a) TG analysis of the Pt/***C***-$(EI)_3$ composite with [Pt]/[N] ratio of 0.13 B, 0.26 C, 0.52 D, and 0.78 E in air. (b) The dependence of real loading percent and efficiency factor on the nominal loading percent.

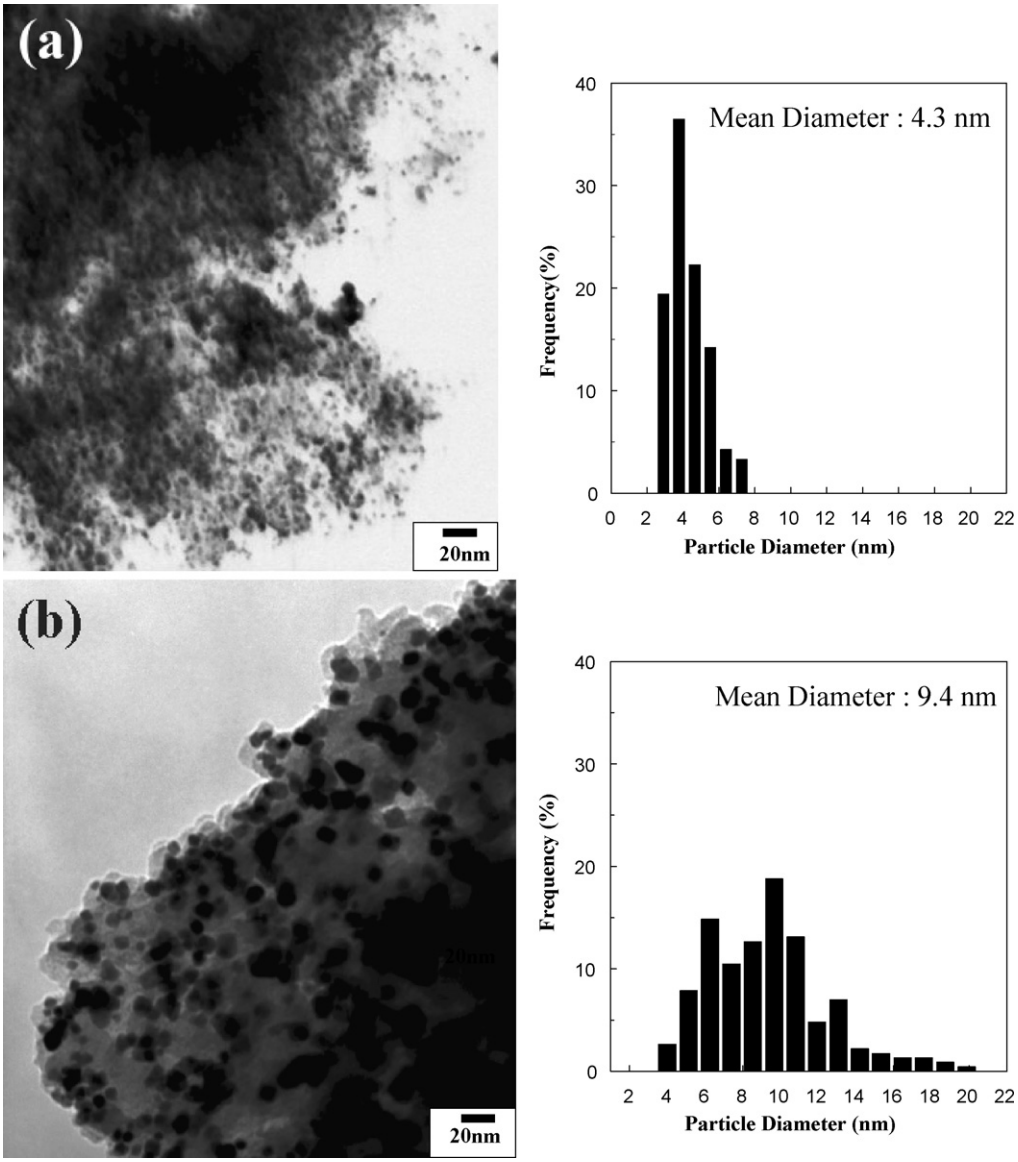

Fig. 8. TEM images and corresponding size histograms of the Pt nanocrystals immobilized on (a) *C*-$(EI)_3$ and (b) HNO_3-treated CNS with the same loading conditions (ω_n = 60 wt.%) after calcination in N_2 at 300 °C for 10 h.

ions in the stock solution that causes the decrease in the loading quantity.

In order to understand the ability of ***C***-$(EI)_3$ in immobilizing Pt, we used the efficiency factor ($\chi = \omega_r/\omega_n$) representing the sequestration characteristics of ***C***-$(EI)_3$, as shown in Table 2. A supplementary sample, **F**, prepared with [Pt]/[N] = 1.04 (ω_n = 80 wt.%) is also shown in Fig. 7b, so as to highlight the inclination of the efficiency curve. An efficiency of 60% for sample **F** was derived and ω_r was determined to be 47.9 wt.%. The morphology of sample **F** is not discussed in this study because the densely layered Pt particles did not permit observation by TEM. In Fig. 7b, the efficiency factor is plotted versus the nominal loading percentage. The efficiency factor decreases exponentially with an increase in the nominal loading percentage. It can be seen that Sample **C** was about 20% more efficient than sample **F**. The efficiency of sample **E** was only 63%, however, it shows a densely loaded structure of finely dispersed 3.5 nm Pt nanoparticles, which may provide a promising material for advanced catalyst applications. The most rational explanation of the decreasing efficiency is the electrostatic repulsion resulting from the immobilized Pt(IV) positive charges, as mentioned above. It may be possible to improve this loading efficiency further by redesigning the molecular structure of the grafted multi-chelates, e.g. by using a longer or dendritic chelating chain, or by using a higher surface area of carbon.

3.4. *Stabilizing effect of* ***C***-*(EI)*$_3$

It is proposed that the presence of ethylenimine chains on the CNS surface can not only stabilize the deposited Pt nanoclusters by the presence of its well-structured amino groups, but that it can also immobilize Pt particles during the calcination process for application in electrochemical devices. Therefore, we further characterized the stability of the densely loaded Pt nanoparticles after thermal treatment. The calcination was performed at 300 °C (this temperature was determined by the thermo-decomposition temperature of ***C***-$(EI)_3$ as shown in Table 1) under a nitrogen atmosphere. Calcination at 300 °C for 10 h did not bring about significant morphological changes, resulting in a [Pt]/[N] ratio of 0.72 (ω_n = 60 wt.%), as shown in Fig. 8a. Finely dispersed Pt nanoparticles with a diameter of ca. 4.3 nm were obtained. As a comparison, the Pt nanoparticles,

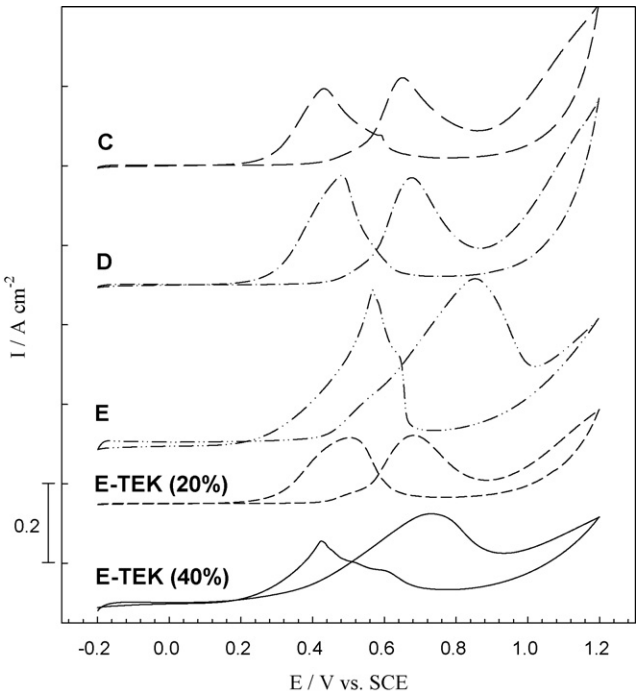

Fig. 9. Cyclic voltammograms of the Pt/***C***-(EI)$_3$ catalysts with [Pt]/[N] ratio of 0.26 C, 0.52 D, and 0.78 E, respectively, as well as the E-TEK catalyst (20% and 40%) in 0.5 M H_2SO_4/1 M CH_3OH at 20 mV s^{-1}.

supported by HNO_3-treated CNS with ω_n = 60 wt.%, were also calcinated under the same condition. As displayed in Fig. 8b, severe coalescence of the particles takes place leading to a significant enlargement of particle sizes (9.4 nm) and a broad size distribution. Based on the above results about calcination, it appears that the steric effects exerted by the grafted ethyleimine chain on the CNS should provide a good protecting effect against the growth of particles during calcination, thereby favoring the formation of small particles with a high degree of uniformity.

3.5. Electrocatalytic activity of the Pt/C-(EI)$_3$ catalysts

It is well known that the functionalization of a catalyst support changes the bulk resistivity of the support which may reduce the activity of the catalyst. In the present study, the samples after calcination were characterized by XPS, and their catalytic activities toward methanol oxidation were measured by cyclic voltammetry. The N 1s line of Pt/***C***-(EI)$_3$ after calcination under N_2 at 300 °C for 10 h is shown in the inset of Fig. 4. The N 1s signal decreases considerably to the level of a trace signal after 10 h suggesting the accomplishing of the removal of the nitrogenous species.

Cyclic voltammetry (CV) was employed to evaluate the activity towards methanol oxidation of the Pt/C catalysts with different loading percentages in an electrolyte containing 0.5 M H_2SO_4/1 M CH_3OH, as displayed in Fig. 9 (−0.2–1.0 V versus SCE, 20 mV s^{-1}). For comparison, the commercial Pt catalysts (E-TEK, 20 and 40 wt.%) were also employed. The voltammetric features are in good agreement with literature, in which the typical methanol oxidation current peak on Pt catalyst is at about 0.71 V versus SCE in the forward scan. The oxidation current increases for all the Pt/C catalysts until the potential reaches 0.71 V and starts to decrease because the formation of Pt oxides inhibits methanol oxidation at this higher potential range. Fig. 9 clearly shows that the oxidation current observed with Pt/C composite **E** is considerably higher than that of the E-TEK 40 wt.% catalyst. This significant improvement in the catalytic performance can be attributed to the high level of dispersion

Table 3
Particle sizes and CV results of the Pt/***C***-(EI)$_3$ catalysts and the E-TEK Pt/C.

Sample	ω_r (wt.%)	Size (nm)[a]	I_f (A mg^{-1} cm^{-2})
C	16.6	4.9	0.37
D	27.5	4.3	0.48
E	37.5	4.3	0.75
E-TEK-20%	19.7	3.2	0.24
E-TEK-40%	38.2	4.2	0.51

[a] Pt particle sizes after calcination.

of Pt nanoparticles on CNTs. The peak current density (I_f) increases from 0.37 to 0.75 A mg^{-1} Pt with the increasing Pt loading percent from 16.6 to 37.5 wt.% as shown in Table 3. There is a shift in the potential at which the peak current arises: 0.71 V for the catalyst **C** and 0.82 V for the catalyst **E**. This shift could result from differences in the distribution of exposed Pt crystal faces exposed on the two samples. The Pt/***C***-(EI)$_3$ catalysts with 37% loading, which possess nanoscopic particle size and high electrocatalytic performance in methanol oxidation, should be a promising candidate for application in fuel cells.

4. Conclusion

The fabrication of densely loaded, nanosized carbon-supported Pt nanoclusters has been demonstrated by using multichelate-functionalized CNSs. The functionalization of the CNSs and the amine value of ***C***-(EI)$_3$ were examined by amine value titrations, TGA and XPS. The N 1s XPS spectra revealed the immobilization of Pt nanoclusters on the CNS surface by Pt–N coordination binding. Finely dispersed and densely loaded Pt clusters (approximately 3.5 nm diameter) were successfully prepared at a [Pt]/[N] ratio of 0.78 (sample **E**), indicating that the grafted ethylenimine chains provide effective steric stabilization through Pt–N binding, which prevents the Pt nanoparticles from aggregating. Moreover, we found that the positive charge resulting from the immobilization of Pt(IV) induced an electrostatic repulsion toward the Pt ions in the stock solution, which, in turn, caused the decrease in the real loading quantity. This effect resulted in the low loading efficiency of 63% for sample **E**. These immobilized Pt nanoclusters did not fuse or coalescence together after firing at 300 °C in N_2 for 10 h, thereby demonstrating the excellent stabilizing effect of the ethylenimine-functionalized CNS. The Pt/***C***-(EI)$_3$ catalyst exhibits an exceptional methanol oxidation activity that is higher than the commercial E-TEK catalyst. For DMFC, a carbon-supported PtRu catalyst could be a more suitable anode material. Efforts are in progress towards improving the stability of the densely loaded catalysts, as well as the synthesizing of densely loaded carbon-supported PtRu.

Acknowledgment

We gratefully acknowledge the National Science Council, Taipei, Taiwan for their generous financial support of this research (NSC 95-2120-M-006-009).

References

[1] J. Zhang, K. Sasaki, E. Sutter, R.R. Adzic, Science 315 (2007) 220–222.
[2] A.S. Arico, S. Srinivasan, V. Antonucci, Fuel Cells 1 (2001) 133–161.
[3] B.C.H. Steele, A. Heinzel, Nature 414 (2001) 345–352.
[4] G.S. Chai, I.S. Shin, J.S. Yu, Adv. Mater. 16 (2004) 2057–2061.
[5] Y. Ding, M. Chen, J. Erlebacher, J. Am. Chem. Soc. 126 (2004) 6876–6877.
[6] M. Neergat, D. Leveratto, U. Stimming, Fuel Cells 2 (2002) 25–30.
[7] D. Zhao, B.-Q. Xu, Angew. Chem. Int. Ed. 45 (2006) 4955–4959.
[8] D.L. Boxall, G.A. Deluga, E.A. Kenik, W.D. King, C.M. Lukehart, Chem. Mater. 13 (2001) 891–900.
[9] S. Liao, K.-A. Holmes, H. Tsaprailis, V.I. Birss, J. Am. Chem. Soc. 128 (2006) 3504–3505.

[10] G. Sakai, T. Yoshimura, S. Isohata, M. Uota, H. Kawasaki, T. Kuwahara, D. Fujikawa, T. Kijima, Adv. Mater. 19 (2007) 237–241.
[11] L. Dai, A.W.H. Mau, Adv. Mater. 13 (2001) 899–913.
[12] Y.-P. Sun, K. Fu, Y. Lin, W. Huang, Acc. Chem. Res. 35 (2002) 1096–1104.
[13] X. Lu, Z. Chen, Chem. Rev. 105 (2005) 3643–3696.
[14] R. Andrews, D. Jacques, D. Qian, T. Rantell, Acc. Chem. Res. 35 (2002) 1008–1017.
[15] R. Shvartzman-Cohen, Y. Levi-Kalisman, E. Nativ-Roth, R. Yerushalmi-Rozen, Langmuir 20 (2004) 6085–6088.
[16] A. Koshio, M. Yudasaka, M. Zhang, S. Iijima, Nano Lett. 1 (2001) 361–363.
[17] J.E. Riggs, Z. Guo, D.L. Carroll, Y.-P. Sun, J. Am. Chem. Soc. 122 (2000) 5879–5880.
[18] W. Huang, S. Fernando, L.F. Allard, Y.-P. Sun, Nano Lett. 3 (2003) 565–568.
[19] J.L. Bahr, J.L. Tour, Chem. Mater. 13 (2001) 3823–3824.
[20] S. Qin, D. Qin, W.T. Ford, J.E. Herrera, D.E. Resasco, S.M. Bachilo, R.B. Weisman, Macromolecules 37 (2004) 3965–3967.
[21] B. Zhao, H. Hu, H.C. Haddon, Adv. Funct. Mater. 14 (2004) 71–76.
[22] R. Blake, Y.K. Gun'ko, J. Coleman, M. Cadek, A. Fonseca, J.B. Nagy, W.J. Blau, J. Am. Chem. Soc. 126 (2004) 10226–10227.
[23] Y. Liu, Z. Yao, A. Adronov, Macromolecules 38 (2005) 1172–1179.
[24] I.-C. Liu, H.-M. Huang, C.-Y. Chang, H.-C. Tsai, C.-H. Hsu, R.C.-C. Tsiang, Macromolecules 37 (2004) 283–287.
[25] (a) M.G.C. Kahn, S. Banerjee, S.S. Wong, Nano Lett. 2 (2002) 1215–1218;
(b) M. Sano, A. Kamino, J. Okamura, S. Shinkai, Langmuir 17 (2001) 5125–5128.
[26] M. Sano, A. Kamino, S. Shinkai, Angew Chem. Int. Ed. 40 (2001) 4661–4663.
[27] L. Cao, W. Yang, J. Yang, C. Wang, S. Fu, Chem. Lett. 33 (2004) 490–491.
[28] P.L. Kuo, S.K. Ghosh, W.J. Liang, Y.T. Hsieh, J. Polymer Sci. Part A: Chem. Ed. 39 (2001) 3018–3023.
[29] P.L. Kuo, S.C. Ni, J. Polym Sci. Part A: Chem. Ed. 42 (2004) 5504–5513.
[30] P.L. Kuo, W.F. Chen, H.Y. Huang, I.C. Chang, S.H.A. Dai, J. Phys. Chem. B 110 (2006) 3071–3077.
[31] C.C. Chen, C.H. Hsu, P.L. Kuo, Langmuir 23 (2007) 6801–6806.
[32] W.F. Chen, H.Y. Huang, C.H. Lien, P.L. Kuo, J. Phys. Chem. B 110 (2006) 9822–9830.
[33] R.V. Hull, L. Li, Y. Xing, C.C. Chusuei, Chem. Mater. 18 (2006) 1780–1788.
[34] C. Gao, C.D. Vo, Y.Z. Jin, W. Li, S.P. Armes, Macromolecules 38 (2005) 8634–8649.
[35] D.Q. Yang, B. Hennequin, E. Sacher, Chem. Mater. 18 (2006) 5033–5038.
[36] J. Li, L. Ma, X. Li, C. Lu, H. Liu, Ind. Eng. Chem. Res. 44 (2005) 5478–5482.
[37] S. Siggia, J.G. Hanna, Quantitative Organic Analysis via Functional Groups, fourth ed., Krieger, Malabar, FL, 1998, pp. 569–572.
[38] M. Peuckert, Electrochim. Acta 29 (1984) 1315–1320.
[39] J.F. Moulder, W.F. Stick, P.E. Sobol, K.D. Bomben, Handbook of X-ray Photoelectro Spectroscopy, PerkinElmer, Eden Prairie, MN, 1992.
[40] J. Sharma, S. Mahima, A.B. Kakade, R. Pasricha, A.B. Mandale, K. Vijayamohanan, J. Phys. Chem. B 108 (2004) 13280–13286.
[41] A. Haimov, H. Cohen, R. Neumann, J. Am. Chem. Soc. 126 (2004) 11762–11763.
[42] A. Adenier, M.M. Chehimi, I. Gallardo, J. Pinson, N. Vila, Langmuir 20 (2004) 8243–8253.
[43] W. Li, C. Liang, W. Zhou, J. Qiu, Z. Zhou, G. Sun, Q. Xin, J. Phys. Chem. B 107 (2003) 6292–6299.
[44] K.W. Park, J.H. Choi, B.K. Kwon, S.A. Lee, Y.E. Sung, H.Y. Ha, S.A. Hong, H.Y. Kim, A. Wieckowski, J. Phys. Chem. B 106 (2002) 1869–1877.
[45] R.M. Crooks, M. Zhao, L. Sun, V. Chechik, L.K. Yeung, Acc. Chem. Res. 34 (2001) 181–190.